IET Power Electronics

IET The Institution of Engineering and Technology WILEY

ORIGINAL RESEARCH PAPER

Four-phase interleaved TCM DC-DC buck converter with matrix inductor in battery charging application

Anh Dung Nguyen[1] | Shu-Xin Chen[2] | Yang Chen[3] | Cheng-Wei Chen[1] | Byeongcheol Han[4] | Jih-Sheng Lai[1]

[1] Future Energy Electronics Center, The Bradley Department of Electrical and Computer Engineering, Virginia Tech, 220 Inventive Ln, Blacksburg, Virginia 24061, USA

[2] Department of Electrical and Electronic Engineering, Nanyang Technological University, 50 Nanyang Avenue, Singapore 639798, Singapore

[3] School of Electrical Engineering, Southwest Jiaotong University, West Section, High-Tech zone, ChengDu, Sichuan 611756, China

[4] School of Electronics Engineering, Kyungpook National University, Daegu 41566, South Korea

Correspondence

Anh Dung Nguyen, Future Energy Electronics Center, the Bradley Department of Electrical and Computer Engineering, Virginia Tech, Blacksburg, Virginia, USA.
Email: adnguyen@vt.edu

Abstract

In this paper, a 1-kW DC-DC buck converter with a four-phase interleaved matrix inductor is proposed for battery charging applications. It is well-known that the DC bias on the inductor will cause high core loss as it changes the B–H characteristic. Typically, the transient conduction mode employed in high voltage applications for zero-voltage-switching of devices would cause higher inductor current ripple. The conventional approach to reduce the effect of DC bias and inductor current ripple is employing multi-phases. However, the cost and size of the converter will increase significantly. This paper proposes the matrix inductor which has a small volume and reduces the effect of the DC bias by flux sharing and flux cancellation at the same time, results in low inductor core loss. With the interleaved operations the output current ripple can be lower which is suitable for battery charging application. Besides, the comparison of the synchronous and interleaved operation is presented. A 1-kW prototype is built and the experimental results show that the peak efficiency is 99.1% and 99.2% for synchronous and interleaved control, respectively. Additionally, the output current ripple of the interleaved operation is reduced by 85% in comparison with the synchronous operation.

1 | INTRODUCTION

Recently, the inductive power transfer (IPT) has been paid more attention due to the advantages, such as safety and convenience, compared to the traditional wired systems. The output load variation and coil misalignment of an IPT system will affect the output stability and overall performance [1, 2]. Several solutions have been presented such as compensation topologies or coil design to reduce the output fluctuation and to achieve constant current or constant voltage output [2–4]. However, the output still varies in a small range because of the unstable control in a wide power range. Thus, it is not appropriate to charge the battery directly [5]. Therefore, the two-stage IPT system which includes the regulated DC-DC buck converter for output battery application has been presented in the literature. In this

approach, the IPT stage can be designed to achieve higher efficiency with wide output variation. The DC-DC buck converter will regulate the output based on the output range of the IPT stage as shown in Figure 1. Thus, the total performance can be improved because of the optimal design of each stage.

In the DC-DC buck converter, under high switching frequencies, the turn-on and turn-off losses are high under hard-switching operation [6–10]. The switching losses are more critical in high voltage applications as the parasitic energy is a square of the voltage. Additionally, the voltage spike caused by hard switching will increase the complexity of the design and devices chosen. Thus, soft-switching has been employed in many applications, such as critical conduction mode (CRM) or transient conduction mode (TCM) [11–15]. However, under CRM/TCM, the magnetic components account for the major
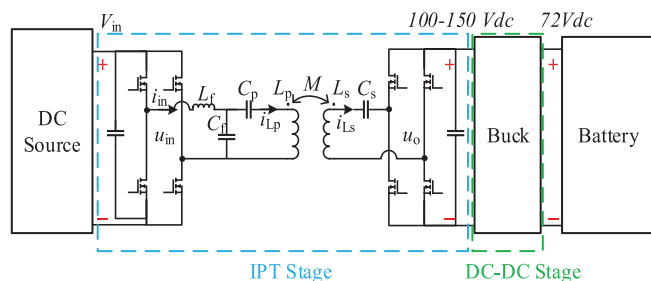
FIGURE 1 Proposed IPT system for battery charging

FIGURE 2 Schematic of four phase DC-DC buck converter

losses in the converter because of higher flux caused by high inductor current ripple [9]. Furthermore, as the switching frequency increases, the design of the inductor is more difficult as it needs to adapt to a wide range of frequency. The high current ripple will limit the design of the core due to size and loss. Two-phase and four-phase interleaved DC-DC converter with inverse coupling and direct coupling are employed to reduce the core loss and winding loss [16–23]. However, the core size is still an issue and the coupling coefficient is not easy to control. Also, due to the wide input range, the switching frequency range of the interleaved structure with coupled inductor will increase significantly because the equivalent inductance is voltage and power dependent, results in higher noise and complexity of the driver design. The effect of DC-bias is another issue [24–26]. The core loss will be higher as the DC-bias increases because it changes the *B–H* characteristic of the core material. Therefore, multi-phases are preferred to reduce the effect of DC-bias and current ripple by sharing the current stress on every phase. However, as the number of phases increases, the difficulty of interleaving the windings will also increase. With the conventional coupled inductor, the interleaved winding from this phase to another phase will make the design more complex, and increases the AC resistance due to longer winding. Furthermore, the total core volume also increases which reduces the efficiency under light load condition. The matrix inductor has been proposed for flux sharing and flux cancellation [27]; thus, the inductor core loss is reduced significantly due to the reduction of DC-bias effect [24–26]. The synchronous operation of the four-phase matrix inductor has been employed for core loss reduction. However, the total current ripple at the output is four times higher than the inductor current of each phase. Thus, the trace copper loss is higher as the RMS current is higher at this point. In addition, the output current ripple is high because of adding ripples of four phases. Therefore, it is not suitable for the battery charger as it will damage the battery.

This paper proposes the interleaved matrix inductor for the four-phase DC-DC buck converter. The matrix inductor has the advantages of flux sharing and flux cancellation, resulting in the reduction of the DC bias effect on inductor core loss. The interleaved operation reduces the output current ripple significantly. The experiment shows that the output current ripple of the interleaved operation is 15% of the synchronous operation. In addition, the analysis and comparison of the interleaved and synchronous operation of matrix inductor are also proposed.
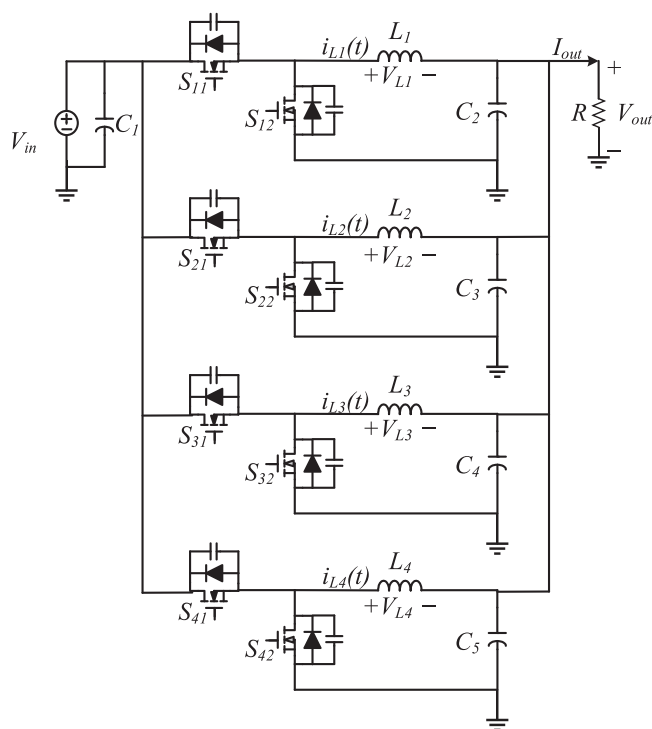
A 1-kW prototype is successfully built and tested to verify the feasibility of the proposed converter.

2 | MATRIX INDUCTOR INVESTIGATION

The inductor current ripple is high in the CRM operation, results in high core loss. The four phases DC-DC buck converter is introduced to reduce the current ripple and DC-bias of the inductor. Figure 2 shows the schematic of the four phases DC-DC buck converter. There are eight switches, four inductors integrated as the matrix inductor, input and output capacitor and terminal.

According to [27], since four phases are employed, the configuration of the inductor can be: (a) four single-core inductors will introduce higher core loss and core volume; (b) two sets of two-phase coupled inductors can reduce the core size with partial flux distribution. However, the inverse coupling will increase the switching frequency range even though it will help for the performance, especially in the wide range voltage applications. Thus, it will increase the complexity of the design of the inductor and driver. Additionally, the inverse coupling will increase the AC flux despite the DC flux is reduced. The direct coupling has an advantage of reducing the AC flux which is suitable for high voltage applications. However, the same to inverse coupling, the winding configuration of the direct coupling is complex which makes the design more difficult. Furthermore, the direct coupling will increase the RMS current which increases the conduction loss, results in lower efficiency. Therefore, this paper proposes the matrix inductor with the advantages of flux
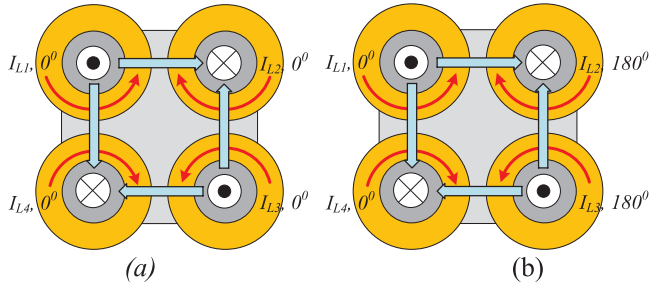
FIGURE 3   Proposed matrix inductor in (a) synchronous and (b) interleaved operation

FIGURE 4   Timing diagrams of (a) synchronous and (b) interleaved operation

sharing and flux cancellation. The flux sharing is applied in the top and bottom plates and flux cancellation is introduced in the middle of two plates. Thus, the core volume and core loss can be reduced significantly because of lower DC and AC flus. By this configuration, the effect of DC-bias on the inductor core loss can be minimized. There are two operations for the matrix inductor as below:

(i) Synchronous operation: four phases of the converter are operated synchronously as shown in Figure 3(a). The flux sharing of conventional E-core can be retained. In addition, the flux cancellation in the centre of the top and bottom plates is achieved. Thus, the core loss can be reduced significantly. However, as four phases are in parallel, the total current ripple is four times higher than one phase. Thus, the high output current ripple will make the converter not suitable for the battery charging application.

(ii) Interleaved operation: the second and the third phases are in 180° phase shift with the first and fourth phase as shown in Figure 3(b). The interleaved structure still keeps the flux sharing and flux cancellation as the synchronous operation. Comparing with the synchronous operation, the output current ripple of the interleaved operation is more than four times smaller because of the TCM operation and the phase shift.

In both configuration, the design of cross-section area of every phase are independent because there is no coupling between phases. Thus, the frequency range of the converter is narrower in comparison with the coupled inductor topology while it still keeps the advantage of lux sharing and flux cancellation.

3 | ANALYSIS OF MATRIX INDUCTOR FOR DC-DC BUCK CONVERTER

In this section, the design and analysis of the matrix inductor in both synchronous and interleaved operation is presented. Figure 4 shows the key waveforms of CRM operation in synchronous and interleaving operations. In order to achieve ZVS for the main switches, the negative current I_0 should be
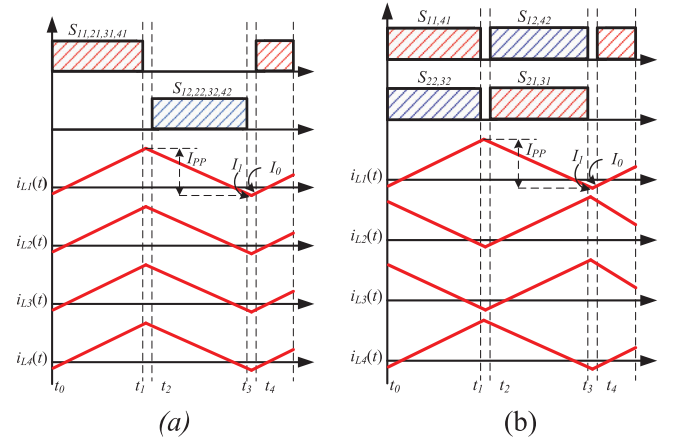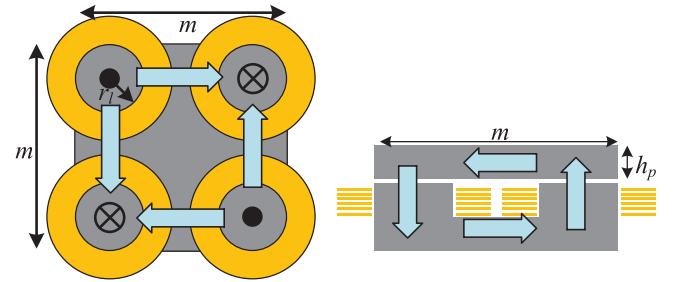
FIGURE 5   Schematic of the proposed matrix inductor

enough to charge and discharge the parasitic capacitance of the MOSFETs. The ZVS condition can be defined according to [10, 27].

$$I_0 > \frac{V_{\text{in}} - V_{\text{out}}\left(1 - \cos\left(\omega_{\text{o}} \cdot t_{\text{d}}\right)\right)}{Z_{\text{o}} \sin\left(\omega_{\text{o}} \cdot t_{\text{d}}\right)} \tag{1}$$

$$Z_0 = \sqrt{\frac{L}{2C_{\text{OSS}}}} \tag{2}$$

$$\omega_{\text{o}} = \frac{1}{\sqrt{2LC_{\text{OSS}}}} \tag{3}$$

where L is the inductance and C_{OSS} is the parasitic capacitance of the MOSFET and t_{d} is the dead-time. The cross section area A_{e} and the air gap g_{a} can be determined according to the inductor current ripple I_{PP}:

$$g_{\text{a}} = \frac{2n}{\Delta H} I_{\text{PP}} \tag{4}$$

$$A_{\text{e}} = \frac{g_{\text{a}}L}{n^2 \mu_0} \tag{5}$$

where n is the number of turns and μ_0 is the permeability.

The schematic of the proposed matrix inductor is presented in Figure 5. As the flux distribution on every leg is Φ, the top
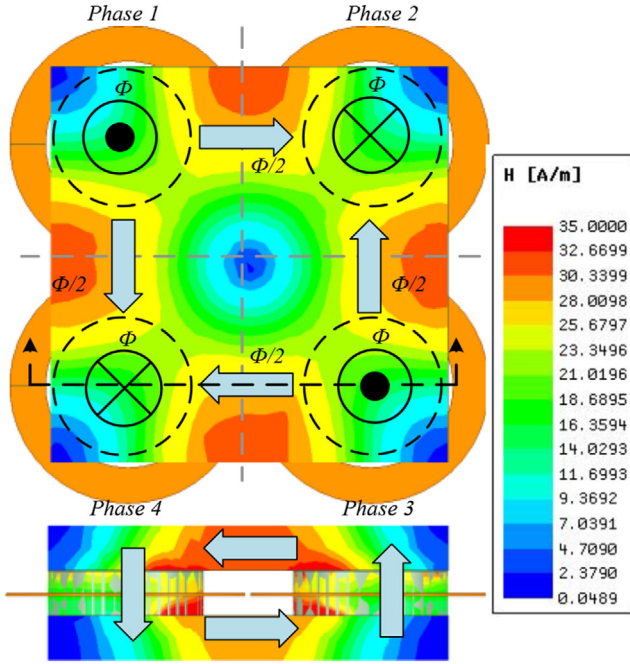
FIGURE 6 Flux distribution of the proposed matrix inductor in synchronous operation

and bottom plates' flux distribution is half of Φ; therefore, the top and bottom plates cross-section area can be defined as:

$$mh_p = A_e = \pi r_1^2 \tag{6}$$

where m is the core length, h_p is the top and bottom plates thickness and r_1 is the leg radius. The flux distribution of the inductor core is shown in Figure 6. There is flux cancellation in the middle of the top and bottom plates whereas the flux sharing is shown in the middle of every two legs.

However, since four-phase are operated in parallel, the output ripple will be high which is not good for battery charging. The interleaved structure is proposed to reduce the ripple. The interleaved operation still keeps the advantage of flux sharing and flux cancellation, as shown in Figure 7. However, the design of the inductor is different from the synchronous operation.

At $t = t_0$, as shown in Figure 7(a), the flux distribution of phase two and three are high (Φ_2) whereas the flux distribution of phase one and four are small (Φ_1) as shown in Figure 8(b). Similarly, at $t = t_1$, as shown in Figures 7(b) and 8(b), the flux distribution of phases one and four is Φ_2 whereas the flux distribution of phases two and three is Φ_1. The maximum flux on the top and bottom plates are determined as:

$$H_{tb} = H_2 - H_1/2 \tag{7}$$

where H_{tb}, H_1 and H_2 are the magnetic field at $t = t_0$ (or $t = t_1$) of top and bottom plates, phase one and phase four (or phase two and phase three) and phase two and phase three (or phase one and phase four), respectively. Thus, the cross-section area

of top and bottom plates A_{tb} can be calculated:

$$A_{tb} = mh_p = \frac{2LI_{PP}}{n\mu_0 H_{tb}}. \tag{8}$$

The inductor voltage waveforms are shown in Figure 8. According to the switching pattern, the inductor voltage can be determined:

$$\begin{cases} V_a = V_{in} - V_{out} \\ V_b = -V_{out} \end{cases} \tag{9}$$

In the synchronous operation, the inductor voltage of four phases are the same. However, phase two and phase three are in 180° phase shift with phase one and phase four in the interleaved operation, the flux will share between them which causes zero coupling coefficient. Thus, the inductor currents of four phases are independent. The AC and DC flux are shown in Figure 9. The flux of each phase can be determined:

$$\begin{cases} \phi_1 = \frac{ni_1}{\mathfrak{R}_1} \\ \phi_2 = \frac{ni_2}{\mathfrak{R}_2} \end{cases} \tag{10}$$

where $\mathfrak{R}_1$ and $\mathfrak{R}_2$ are the magnetic reluctance values of four legs and can be expressed as:

$$\mathfrak{R}_{1,2} = \sum \frac{l}{\mu_r A_e} \tag{11}$$

where μ_r is the corresponding permeability of materials in the flux path and l is the length of the magnetic flux path. Because of non-coupled inductor, four phases of the matrix inductor can be considered independently even though it still employs the flux sharing and flux cancellation. Thus, the design of the inductor is easier in comparing with the coupled inductor.

Figure 10 shows the analysis of the output current ripple of the synchronous and interleaved operation of four-phase matrix inductor. as four phases are operated in parallel, the output ripple is four times higher than each phase. However, the interleaved operation can reduce the output ripple because of the phase shift. The frequency of the ripple is two times higher than the switching frequency; however, the magnitude of the ripple is more than four times smaller than the synchronous operation.

4 | EXPERIMENTAL RESULTS

To verify the proposed DC-DC buck converter with matrix inductor, a 1-kW prototype is built and tested. The specification of the power stage is given in Table 1. The input of the DC-DC buck converter is the output of the IPT stage whereas the output is the battery. The relationship between switching frequency range and output power is shown in Equations (12–14) and Figure 11. The inductance of 8uH is chosen for the range
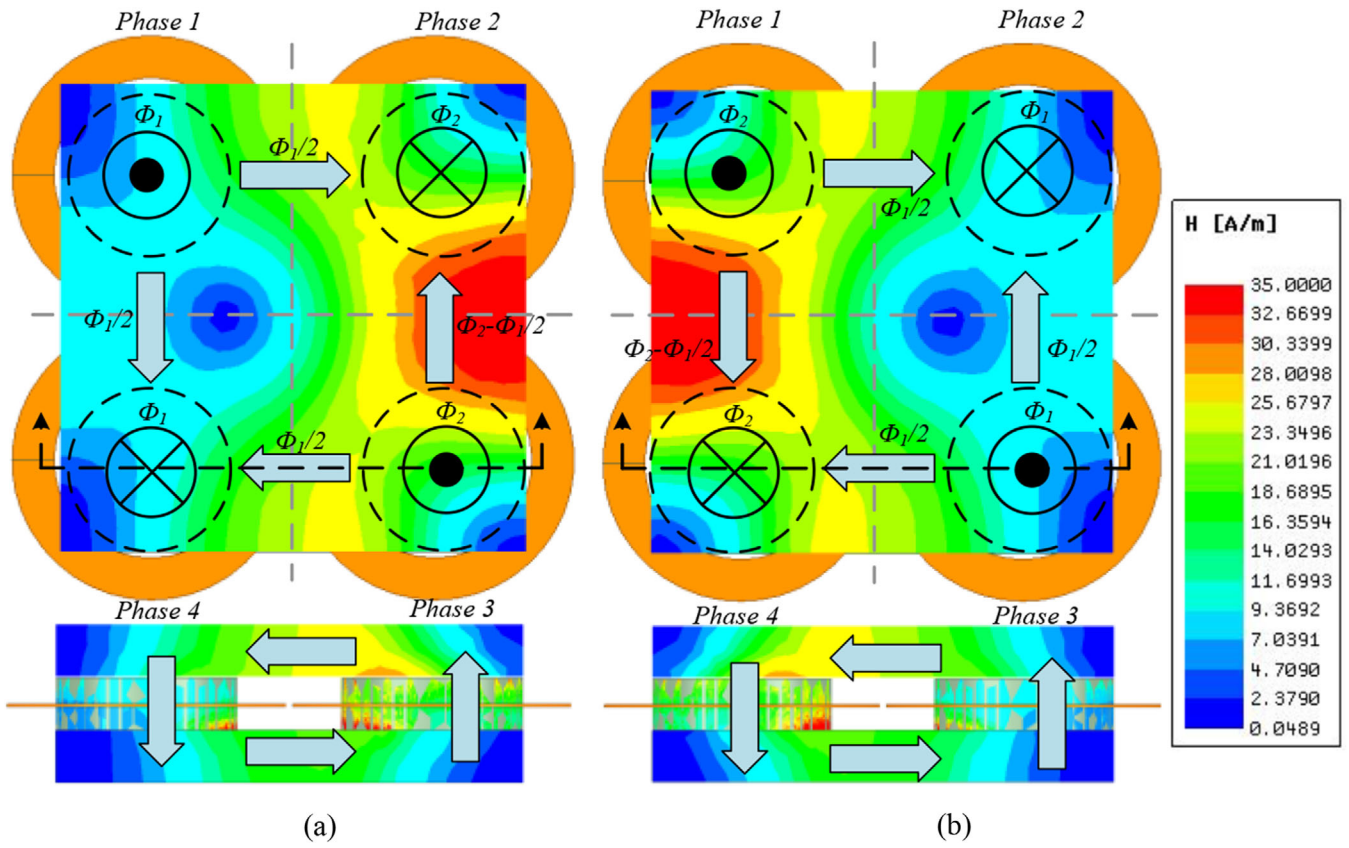
FIGURE 7 Flux distribution of the proposed matrix inductor in interleaved operation at (a) $t = t_0$ and (b) $t = t_1$
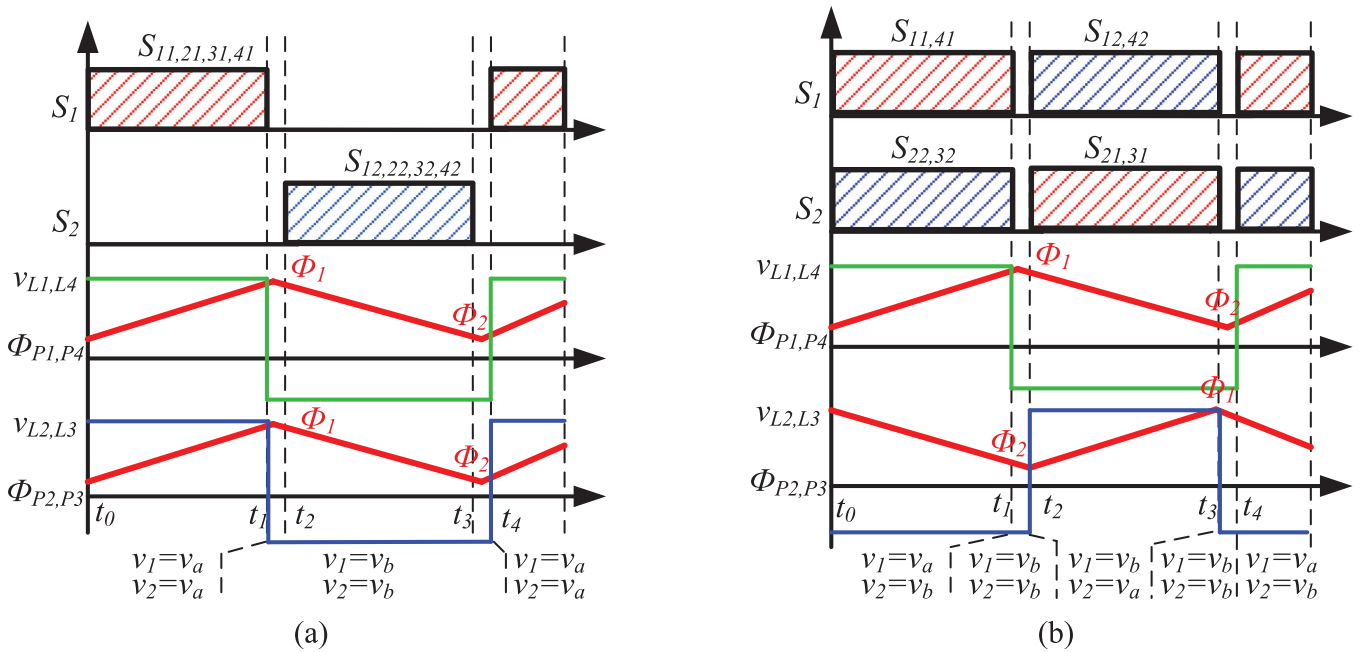

FIGURE 8 Inductor voltage waveforms (a) synchronous and (b) interleaved operation
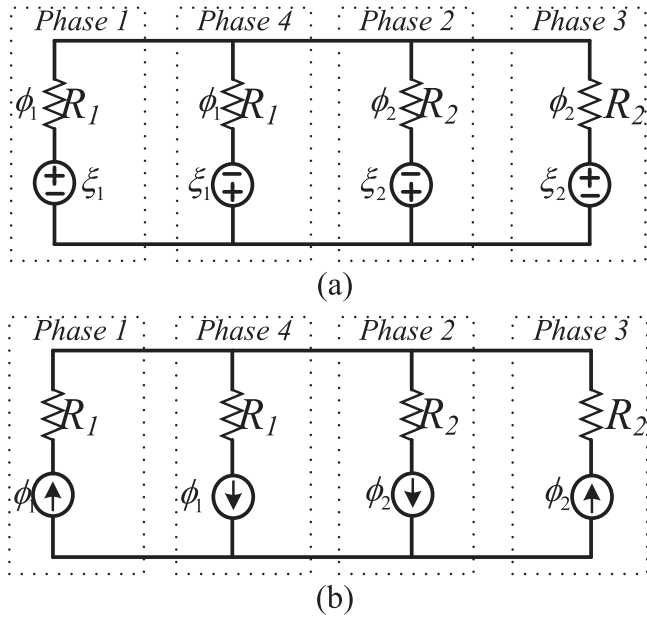
FIGURE 9 Simplified magnetic circuit for (a) DC and (b) AC flux analysis
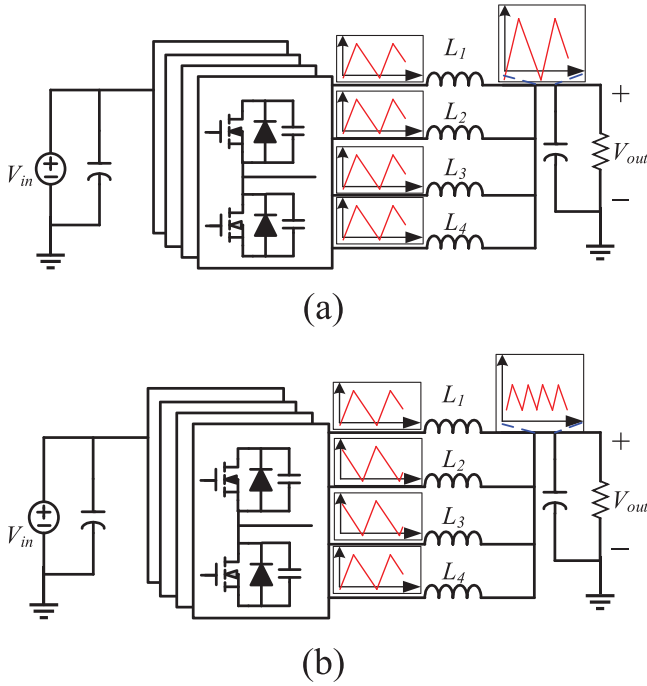

FIGURE 10 Output current ripple of (a) synchronous and (b) interleaved operation

TABLE 1 Specifications of the Proposed DC-DC Buck Converter

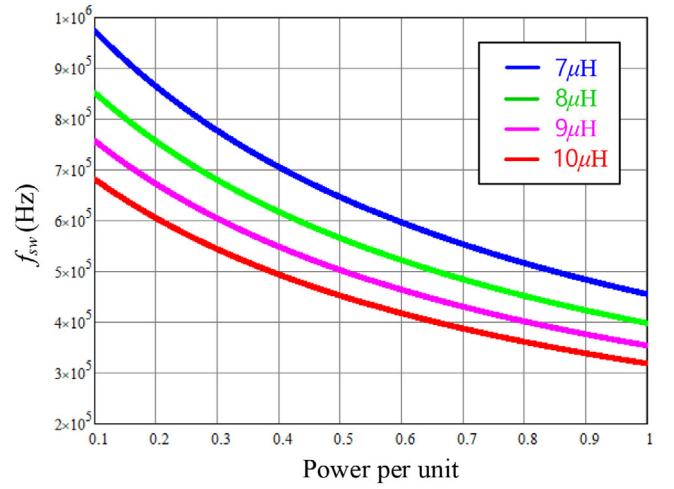| Parameter	Value
Input voltage, V_{in}	100–150 V_{dc}
Output voltage, V_{out}	72 V_{dc}
Rated power, P_o	1000 W
Frequency range	>250 kHz
Devices, S_{11-44}	BSC220N20SFD
Output capacitance, C_{2-5}	176 µF
Core material	ML91S
Inductance, L_{1-4}	8 µH

FIGURE 11 Relationship between switching frequency and output power with different inductance

of the switching frequency of 370 to 840 kHz, and the MOSFET from Infineon (BSC220N20NSFD) is adopted due to its low parasitic. According to Equation (1), the required current for ZVS condition of the switches is 1.25A. the negative current is chosen at 2A for ZVS condition because of layout and devices parasitic.

$$t_{on}(V_{in}, V_{out}, I_{out}) = \frac{2L}{V_{in} - V_{out}}(I_0 + I_{out}) \qquad (12)$$

$$t_{off}(V_{in}, V_{out}, I_{out}) = \frac{2L}{V_{out}}(I_0 + I_{out}) \qquad (13)$$

$$f_{SW}(V_{in}, V_{out}, I_{out}) = \frac{1}{t_n(V_{in}, V_{out}, I_{out}) + t_{off}(V_{in}, V_{out}, I_{out})} \qquad (14)$$

The experimental waveform of the proposed DC-DC buck converter with matrix inductor is shown in Figure 12 when the input voltage is 100 V_{dc}. Figure 12(a,b) show the waveform in synchronous mode whereas Figure 12(c,d) shows the waveform in interleaved mode. The inductor current of phase two and three are always in 180° phase-shift with the inductor current of phase one and four in the interleaved operation. Figure 13 shows the inductor current waveform at 150 V_{dc} input voltage.

Figure 14 shows the output current ripple of the converter in both synchronous and interleaved operation at 20% power. According to the analysis and the experimental results, the output ripple of the interleaved operation is 85% smaller than the synchronous operation. Thus, it is not only suitable for the battery charging applications but also can reduce the output bulk capacitance which reduces the size and cost significantly. The overall performance of the proposed converter is shown in Figure 15 (Pu: power per unit). The experiment shows that the peak efficiency is 99.1% and 99.2% for the synchronous and interleaved operation, respectively. The loss breakdown of the converter at 100 V_{dc} input/1 kW is shown in Figure 16. Figure 17
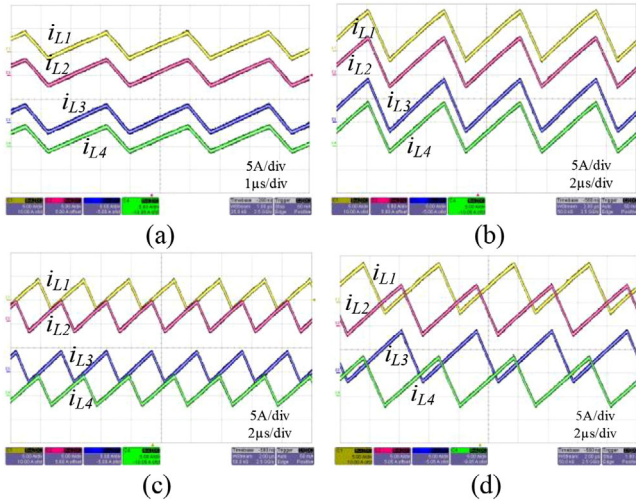
FIGURE 12 Experimental waveforms at 100 V_{dc} input in (a,b) synchronous operation and (c,d) interleaved structure at 20% and 100% load, respectively
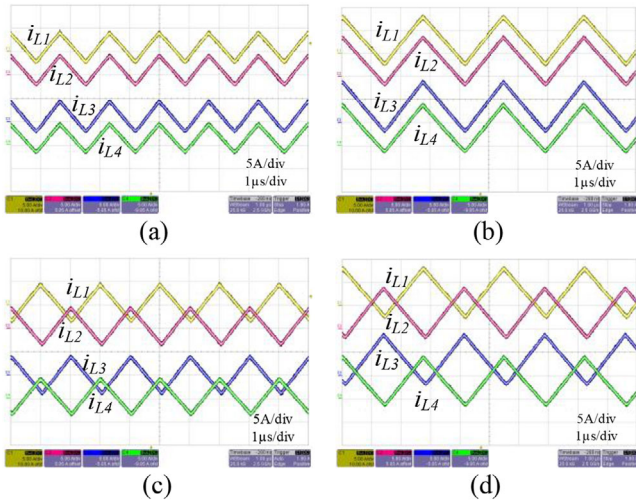

FIGURE 13 Experimental waveforms at 150 V_{dc} input in (a,b) synchronous operation and (c,d) interleaved structure at 20% and 100% load, respectively

shows the prototype of the proposed matrix inductor with four phases DC-DC buck converter.

5 | CONCLUSION

This paper proposed the four-phase interleaved DC-DC buck converter with a matrix inductor for battery charging applications. The proposed matrix inductor has the advantage of flux sharing and flux cancellation. Thus, the effect of DC-bias on the inductor is reduced significantly, results in lower core loss. This paper also presents and compares the different operations of the matrix inductor. The synchronous operation can help to balance the flux distribution. However, the output ripple is high which causes higher AC loss because of higher RMS current.
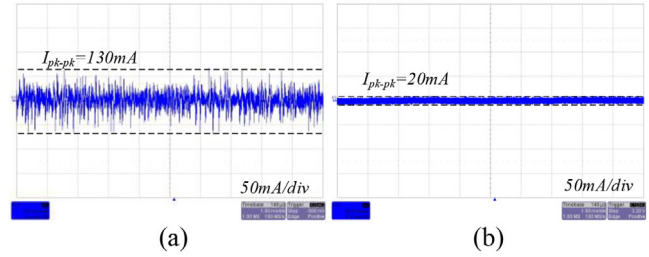

FIGURE 14 Output current ripple of (a) synchronous and (b) interleaved operations
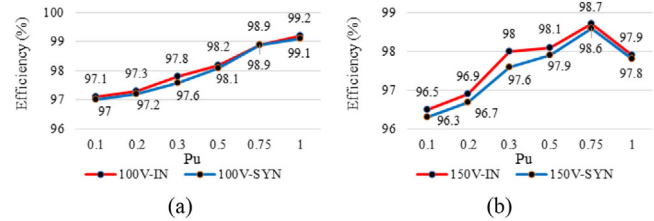

FIGURE 15 Overall performance of (a) 100 V_{dc} and (b) 150 V_{dc} input (-IN: interleaved, -SYN: synchronous)

Additionally, the high output ripple is not suitable for battery charging application. To reduce the output ripple significantly, the interleaved operation with 180° phase shift was proposed with a matrix inductor. A 1-kW prototype was built and tested to verify the feasibility of the proposed converter. The results
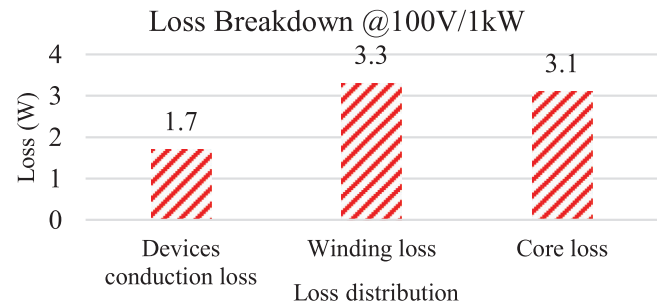

FIGURE 16 Loss breakdown of the converter @100 V_{dc} input/1 kW

FIGURE 17 Prototype of the proposed DC-DC buck converter

showed that the peak efficiency of the interleaved operation was 99.2% and its output current ripple was reduced to 15% of that in the synchronous operation.

ACKNOWLEDGEMENTS

ORCID

Anh Dung Nguyen ⓘ https://orcid.org/0000-0002-1129-1187
Yang Chen ⓘ https://orcid.org/0000-0003-3868-3145
Byeongcheol Han ⓘ https://orcid.org/0000-0001-7770-2025

REFERENCES

1. Dai, J., et al.: A survey of wireless power transfer and a critical comparison of inductive and capacitive coupling for small gap applications. IEEE Trans. Power Electron. 30(11), 6017–6029 (2015)
2. Lu, F., et al.: An inductive and capacitive combined wireless power transfer system withlc-compensated topology. IEEE Trans. Power Electron. 31(12), 8471–8482 (2016)
3. Diekhans, T., et al.: A dual-side controlled inductive power transfer system optimized for large coupling factor variations and partial load. IEEE Trans. Power Electron. 30(11), 6320–6328 (2015)
4. Ju, X., et al.: Switching technique for inductive power transfer at high- Q regimes. IEEE Trans. Indust. Electron. 62(4), 2164–2173 (2015)
5. Uddin, K., et al.: The effects of high frequency current ripple on electric vehicle battery performance. Appl. Energy 178, 142–154 (2016)
6. Chen, Y., et al.: Comparative analysis of power stage losses for synchronous Buck converter in Diode Emulation mode vs. Continuous Conduction Mode at light load condition. In: 2010 Twenty-Fifth Annual IEEE Applied Power Electronics Conference and Exposition (APEC), pp. 1578–1583. Palm Springs, CA, (2010)
7. Ayachit, A., et al.: Averaged small-signal model of PWM DC-DC converters in CCM including switching power loss. IEEE Trans. Circuits Syst. Express Briefs 66(2), 262–266 (2019)
8. Gamand, F., et al.: A 10-MHz GaN HEMT DC/DC boost converter for power amplifier applications. IEEE Trans. Circuits Syst. Express Briefs 59(11), 776–779 (2012)
9. Yahaya, N. Z., et al.: Experimental analysis of a new zero-voltage switching synchronous rectifier buck converter. IET Power Electron. 4(7), 793–798 (2011)
10. Kondrath, N., et al.: Control-to-output transfer function of peak current mode controlled pulse-width modulated DC–DC buck converter in continuous conduction mode. IET Power Electron. 5(5), 582–590 (2012)
11. Liu, Y., et al.: High switching frequency TCM digital control for bidirectional interleaved buck converters without phase error for battery charging. IEEE J. Emerg. Sel. Top. Power Electron. 8, 2111–2123 (2020)
12. Liu, Z., et al.: High-efficiency high-density critical mode rectifier/inverter for WBG-device-based on-board charger. IEEE Trans. Indust. Electron. 64(11), 9114–9123 (2017)
13. Chen, H., et al.: High-efficiency PFM boost converter with an accurate zero current detector. IEEE Trans. Circuits Syst. Express Briefs 65(11), 1644–1648 (2018)
14. Liu, Z., et al.: Design of GaN-based MHz totem-pole PFC rectifier. IEEE J. Emerg. Sel. Top. Power Electron. 4(3), 799–807 (2016)
15. Yang, F., et al.: Interleaved critical current mode boost PFC converter with coupled inductor. IEEE Trans. Power Electron. 26(9), 2404–2413 (2011)
16. Eskandarpour Azizkandi, M., et al.: Two- and three-winding coupled-inductor-based high step-up DC–DC converters for sustainable energy applications. IET Power Electron. 13(1), 144–156 (2020)
17. Pajnić, M., et al.: Design and analysis of a novel coupled inductor structure with variable coupling coefficient. IET Power Electron. 11(6), 961–967 (2018)
18. Yu, D., et al.: Pulse train controlled buck converter with coupled inductors. IET Power Electron. 10(10), 1231–1239 (2017)
19. Yang, Y., et al.: A comprehensive analysis of coupled inductors in 4 phases interleaving bidirectional DC/DC converter. In: 2012 3rd IEEE International Symposium on Power Electronics for Distributed Generation Systems (PEDG), pp. 603–607. Aalborg (2012)
20. Fu, M., et al.: Optimal design of planar magnetic components for a two-stage GaN-Based DC–DC converter. IEEE Trans. Power Electron. 34(4), 3329–3338 (2019)
21. Huber, L., et al.: Open-loop control method for interleaved DCM/CCM boundary boost PFC converter. IEEE Trans. Power Electron. 23(4), 1649–1657 (2008)
22. Xu, X., et al.: Two-phase interleaved critical mode PFC boost converter with closed loop interleaving strategy. IEEE Trans. Power Electron. 24(12), 3003–3013 (2009)
23. Marvi, F., et al.: Zero voltage switching interleaved coupled inductor synchronous buck converter operating at boundary condition. IET Power Electron. 9(1), 126–131 (2016)
24. Muhlethaler, J., et al.: Core losses under the DC bias condition based on steinmetz parameters. IEEE Trans. Power Electron. 27(2), 953–963 (2012)
25. Roshen, W. A., A practical, accurate and very general core loss model for nonsinusoidal waveforms. IEEE Trans. Power Electron. 22(1), 30–40 (2007)
26. Brockmeyer, A., Experimental evaluation of the influence of DC-premagnetization on the properties of power electronic ferrites. In: Proceedings of Applied Power Electronics Conference. APEC '96, pp. 454–460. San Jose, CA (1996)
27. Nguyen, A. D., et al.: Matrix inductor with DC-bias effect reduction capability for GaN-based DC-DC boost converter. IEEE Trans. Circuits Syst. II Express Briefs 67, 2597–2601 (2019)